Evaluation of radome effects on the radiation properties for a 24 GHz phased array antenna

ATEFEH MOUSAVI
MASTER´S THESIS
DEPARTMENT OF ELECTRICAL AND INFORMATION TECHNOLOGY
FACULTY OF ENGINEERING | LTH | LUND UNIVERSITY

Evaluation of radome effects on the radiation properties for a 24 GHz phased array antenna

Atefeh Mousavi
Soc15am1@eit.lth.se

Department of Electrical and Information Technology
Lund University

Supervisor:
Daniel Sjöberg
Andreas Glatz

Examiner:
Mats Gustafsson

June 26, 2020

Printed in Sweden
Tryckeriet i E-huset, Lund

Abstract

A radome is a structural, often waterproof, enclosure in front of an antenna to protect it from external environmental disturbance. The vital role of a radome is to protect the antenna from the effects of the surroundings with minimal impact on the antenna performance. The radome is designed to be transparent to radar and radio waves. The geometry of the radome causes several effects on the electromagnetic performance. Thus, a radome must be designed attentively to certify that it has least impact on radiation and electrical performance of the enclosed antenna. The methodology used in this project is to measure the distortion effect by evaluating the Bore Sight Error (BSE), which shows the deviation of the direction of the antenna main lobe when the radome is introduced around the antenna. The approach used in this thesis is a full wave simulation of a two-dimensional radome and an antenna capable of steering its beam, computed using the Comsol Multiphysics software. The radome is designed for a 24 GHz antenna with different geometries and various parameters.

Keyword: radome, boresight error (BSE), radar, antenna, 24 GHz antenna, phased array antenna, flat radome, curved radome.

Acknowledgements

I would like to express my deepest gratitude to my supervisor Daniel Sjöberg for his invaluable support and advise throughout the period of working on this thesis. He has provided a constant encouragement and careful monitoring despite of the difficult situation caused by COVID-19 virus when the university were closed and access to him was not feasible.
The opportunity I had to work with Andreas Glatz was a great chance for learning and professional development. I express my deepest thanks to him who in spite of being very busy in his duties, took time to guide me and arrange facilities to make this study easier.
Finally I would like to thank my husband Behzad, my sister Arefeh and my whole family for their support and patience throughout my studies. I perceive as this opportunity as a big milestone in my study and career development.

Popular Science Summary

In the modern society, we are using electromagnetic waves to transmit and receive information and energy wireless daily and maybe most of us never think about it. Some everyday examples are smartphones, car remote controls, some kids toys etc. To use these, we need a device to convert electric current to electromagnetic waves, which is called an antenna. An antenna is designed to send and receive electromagnetic waves sometimes thousands of kilometers around the earth or even in space. It can be implemented in radar systems to detect an object's range, direction and velocity. The radar antenna needs protection from the surrounding environment such as rain, wind, dust.etc. The protection device is called a radome. The radome should be as transparent as possible to electromagnetic radiation to induce less impact on electromagnetic waves. However, transparency is not easily achievable since the radome needs to be structurally strong at the same time. For example, the radome must be robust to resist powerful mechanical conditions such as rain and wind and should simultaneously be light weight. For different purposes, there are different factors to design and manufacture a radome and all these requirements can not be fully satisfied at the same time. This means that the electrical transparency will be affected, that is to say, the radome will to some extent change and effect the antenna performance. By considering the radome design purposes, there are some important parameters to evaluate the radome effect on antenna performance such as how much deviation will accrue when the radome is in place or how much antenna power will be lost or how much distortion happens in the radiation pattern. In this study we explain how the radome geometry can affect the antenna. By using Comsol Multiphysics software, different geometries for the radome are simulated and their effect on different antenna models is investigated to define the impact of this type of radome on these antenna. A certain radome material and frequency are considered to study. In this thesis, deviation of propagation and power loss of antenna are important. In other words, a change of propagation direction means that the object appears to be in a different direction than it really is, and a power loss means that we may have smaller range of detecting the objects. Therefore, the deviation and gain were calculated in different designs to study the radome effect on antenna.

Table of Contents

1 Introduction **1**
- 1.1 Background . . . 1
- 1.2 Thesis goal . . . 2
- 1.3 The outline of this thesis . . . 2

2 Fundamentals of Radomes **3**
- 2.1 Radome definition . . . 3
- 2.2 Radome effects on antenna performance . . . 4
- 2.3 Radome Calculations . . . 5

3 Implementation of Radome **9**
- 3.1 Parameters . . . 9
- 3.2 Geometry . . . 10
- 3.3 Antenna configuration . . . 10
- 3.4 Evaluation method . . . 11

4 Flat radome geometry **13**
- 4.1 Flat radome effect on a single-port antenna . . . 14
- 4.2 Flat radome effect on an array-dipole antenna . . . 19

5 Curved radome geometry **21**
- 5.1 Curved radome effect on a single-port antenna . . . 21
- 5.2 Curved radome effect on an array-dipole antenna . . . 26

6 Discussion and conclusion **29**

7 Future Work **33**

A Radiation pattern plots **35**

List of Figures

2.1 Radome configurations: a) electrically thin, b) half-wave, c) A-sandwich, d) B-sandwich, e) C-sandwich, f) multilayer. 4
2.2 Reflection-transmission through a dielectric slab at normal incidence. Only the first two internal propagations are indicated. 6
2.3 Reflection-transmission through a dielectric slab at an oblique incident angle. 6

3.1 Two different geometries for radomes. 10
3.2 Array dipole antenna. 11
3.3 Graphic representation of Boresight error. 11

4.1 Figure shows D and R that are changed to evaluate different designs. 13
4.2 Different edge shapes for the flat radome. 14
4.3 BSE of different alternatives of flat radome (single-port antenna) in z-component. 15
4.4 BSE of different alternatives of flat radome (single-port antenna) in x-component. 16
4.5 Gain of different alternatives of flat radome (single-port antenna) for z-component. 17
4.6 Gain of different alternatives of flat radome (single-port antenna) for x-component. 17
4.7 Reflection coefficient of different alternatives of flat radome (single-port antenna) for z-component. 18
4.8 Reflection coefficient of different alternatives of flat radome (single-port antenna) for x-component. 18
4.9 BSE of different alternatives of flat radome (14-array-dipole antenna) for z-component 19
4.10 BSE of different alternatives of flat radome (14-array-dipole antenna) for x-component 20

5.1 Geometry and parameters D and R for curved radome designs. 21
5.2 BSE of different alternatives of curved radome (single-port antenna) in z-component. 22

5.3 BSE of different alternatives of curved radome (single-port antenna) in x-component. 23
5.4 Gain of different alternatives of curved radome (single-port antenna) in z-component. 24
5.5 Gain of different alternatives of curved radome (single-port antenna) in x-component. 24
5.6 Reflection coefficient of different alternatives of curved radome (single-port antenna) in z-component. 25
5.7 Reflection coefficient of different alternatives of curved radome (single-port antenna) in x-component. 25
5.8 BSE of different alternatives of curved radome (14-array-dipole antenna) in z-component. 26
5.9 BSE of different alternatives of curved radome (14-array-dipole antenna) in x-component. 27

A.1 Radiation pattern plots of different alternatives of flat radome (single-port antenna) beam-steering angle 70 degree in z-component. . . . 36
A.2 Radiation pattern plots of different alternatives of flat radome (single-port antenna) beam-steering angle 70 degree in x-component. . . . 37
A.3 Radiation pattern plots of different alternatives of flat radome (array-dipole antenna) beam-steering angle 70 degree in z-component. . . 38
A.4 Radiation pattern plots of different alternatives of flat radome (array-dipole antenna) beam-steering angle 70 degree in x-component. . . 39
A.5 Radiation pattern plots of different alternatives of curved radome (single-port antenna) beam-steering angle 70 degree in z-component. 40
A.6 Radiation pattern plots of different alternatives of curved radome (single-port antenna) beam-steering angle 70 degree in x-component. 41
A.7 Radiation pattern plots of different alternatives of curved radome (array-dipole antenna) beam-steering angle 70 degree in z-component. 42
A.8 Radiation pattern plots of different alternatives of curved radome (array-dipole antenna) beam-steering angle 70 degree in x-component. 43

List of Tables

3.1 Parameters of the radome and antenna design. *The PML is a fictitious layer absorbing all outgoing waves, whereas the far field surface is where the fields are recorded and subsequently transformed to far field data by Comsol. 9

4.1 Table of different values for two parameters D and R (Flat radome). $d = 2\lambda$ and $r = \lambda$. 13

5.1 Table of different values for two parameters D and R (curve radome with a single-port antenna) $d = 2\lambda$ and $r = \lambda$. 21

Chapter 1
Introduction

Radio Detection and Ranging (RADAR) system is an electromagnetic system used to detect objects by means of radio waves. A radar determines observation angle, velocity, and range of objects and it can be used to detect aircrafts, ships, motor vehicles, etc. The location and speed of an object are determined when radio waves are sent by a transmitter and the reflected signal is collected from the object by the receiver. Radome is a portmanteau word of radar dome, and is a mechanical device to protect the antenna against environmental conditions such as wind, rain, ice, freezing rain, etc. The radome needs to be transparent at the operating band of the radar to minimally attenuate the electromagnetic signal transmitted or received by the antenna. In order to design a radome, geometrical shape (such as a nose cone, flat slab or spherical structure), material, mechanical properties and effects of the radome on the transmitted or received signals should be considered depending on the application of interest [1]. The definition of a suitable geometry shape is a critical part of a radome's design. In addition to shape design, to find an efficient radome design, other parameters such as thickness of the radome, the permitivitty and the radome wall distance from the antenna should be considered. The presence of the radome to an antenna system causes the loss and distortion of the radiation pattern and will change the radiation pattern from the look angle of the antenna. The degradation effect studied in this project is that of Bore Sight Error (BSE). BSE is an important parameter in evaluating the radome performance. The motivation of the thesis is to design a radome that minimizes the affect of the radome on antenna performance and optimizes the angle accuracy of a radar system.

1.1 Background

The study of radomes was intensified in 1940 due to the development of microwave radar on higher speed aircraft [2]. Some examples of using radomes on the equipment are military radar, telecommunication, microwave, civil and military, flight simulation, weather radar, security camera etc [3]. A simple radome is made from a flat dielectric slab, one-half wavelength in thickness. In one study, the thickness of radome layer was adjusted to optimize the radome performance [4]. They used simulation to find the best thickness profile to reduce the maximum BSE as much as possible. In another approach, a genetic algorithm in combination with a

ray tracing method was used to optimize the BSE when the thickness of the skin and the core layer of the radome were optimization parameters [5]. The material properties of the radome were also investigated to improve the electromagnetic performance of the radome [6]. In this thesis, the radome shape and geometrical designs are parameters to optimize the radome performance.

1.2 Thesis goal

This project aims to investigate, design and evaluate different shapes of radomes to analyze and find the best geometry to keep minimum signal attenuation or signal losses and also minimize BSE and distortion of the radiation pattern when covering a 24 GHz antenna. The simulation was done in this thesis by Comsol Multiphysics. The outcome of the project is to propose a design guideline for the radome to get sufficient beam and decrease BSE and also the radome should cause minimum attenuation and affect the antenna signal performance as little as possible. This guideline shows how changing parameters of the radome geometry affects the antenna performance.

1.3 The outline of this thesis

This thesis is outlined as follow. Chapter 2 provides a literature review of radomes, important antenna parameters and error measures which are affected by enclosing the antenna with a radome. The calculation of basic radome parameters is presented at the end. In Chapter 3, all parameters and geometries for the design of a suitable radome for this thesis are explained. Furthermore, an evaluation method for these designs is described. Chapter 4 presents the methodology of different alternative designs of flat radome geometry with changing two parameters of distance between antenna and top of radome and edge of radome in ground plane for two different antenna models: a single-port antenna and a 14-array-dipole antenna. Chapter 5 presents a radome design which is named curved radome in this thesis with similar antennas model as used in Chapter 4 for evaluation. Discussion and conclusions are presented in Chapter 6. At the final chapter, some possible future work in this field is outlined.

Chapter 2

Fundamentals of Radomes

2.1 Radome definition

A radome is a dome-shaped housing for supporting a radar antenna. While the radome protects the antenna from the environment, it also causes transmission interference. The influence of the radome cover on radiation characteristics can be reduced with an efficient radome design [7] [8]. Minimum reflections at the surface of the cover and maximum transmission are desirable. Some important definitions of radome and antenna which should be known to design are explained briefly in this chapter.

2.1.1 Radome material

Choosing the radome material depends on the application and should usually be waterproof and electrically isolating [9]. Two main electromagnetic properties of radome materials are the dielectric constant ε (permittivity), which often increases when the density of the material increases, and the loss tangent $\tan\delta$, which expresses the ratio of the loss of electric energy. Thus, by considering the radome weight, the permittivity should be as small as possible, and considering the radome insertion loss, the loss tangent should be as small as possible. The dielectric constant is one of the most important parameters in order to calculate the optimal thickness.

2.1.2 Radome configuration

There exist several different configurations for radomes: single-layer (electrically-thin and half-wave) and multilayer (A-sandwich, C-sandwich, and others) configurations. For a single layer structure, the layer thickness in an electrically-thin radome is less than 0.1λ and for half-wave radome equals 0.5λ at the frequency of interest. In a multilayer radome, there are different configurations consisting of a combination of two or more layers with different dielectric constant. All different structures are shown in Figure 2.1 [10].

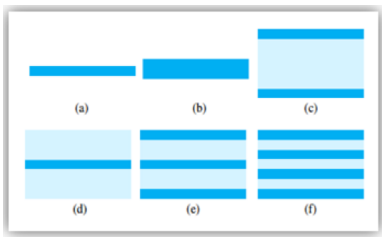

Figure 2.1: Radome configurations: a) electrically thin, b) half-wave, c) A-sandwich, d) B-sandwich, e) C-sandwich, f) multi-layer.

2.1.3 Insertion Loss

Insertion loss is the amount of total power loss due to reflection and absorption by the radome when the electromagnetic wave propagates through the radome material. Insertion loss depends crucially on $\tan\delta$ [11].

2.2 Radome effects on antenna performance

To design and analyze a radome, an antenna and radome should be considered together as a system. The influence of the radome on the antenna performance, such as gain, sidelobe level, beamwidth, polarization, etc, needs to be investigated.

2.2.1 Boresight Error (BSE)

Introducing a radome to an antenna causes distortion of the electromagnetic wavefront through the dielectric material and it makes an angular deviation of the main beam from boresight of the intended angle which is known as boresight error (BSE) [12]. BSE is one of the most important parameters to determine the radome performance and is necessary to determine the required manufacturing tolerance [13].

2.2.2 Gain

The gain of an antenna is defined as the ratio of the power density of an antenna's radiation pattern when it propagates in the direction of the strongest radiation to that of a reference antenna. In this thesis, the reference antenna is an isotropic radiator, which is a fictitious antenna radiating equally in all directions [14] [15].

2.2.3 Sidelobe Degradation

By introducing the radome, the antenna sidelobes will change because of distortion and transmission effects. The radome may make extra sidelobes for some low sidelobe antennas [13].

2.2.4 Pattern and polarization distortions

Another effect of the radome on the antenna performance is deviation or change of the main lobe's direction and shape. Change in direction is BSE, change in amplitude is gain and change in shape is mostly beam width. It also may cause an increase in side lobes and cross-polarization.

2.3 Radome Calculations

Manufacturing a radome with good transparency to the desired radio frequency is possible by using a material with a low dielectric constant (relative permittivity). Using materials with low relative permittivity causes a reduction in reflection. This is due to the different impedance of the free space and the dielectric material. These types of material have minimum effects on radiation pattern and insertion loss. The impedance of a material is stated by (2.1) [16]:

$$Z = \sqrt{\frac{\mu}{\varepsilon}} = \sqrt{\frac{\mu_0 \mu_r}{\varepsilon_0 \varepsilon_r}} \tag{2.1}$$

where:
Z = impedance
μ = permeability
μ_0 = permeability of free space
μ_r = material relative permeability
ε = dielectric constant
ε_0 = dielectric constant of free space
ε_r = relative dielectric constant of material

As previously mentioned, there are different styles of constructing a radome wall known as solids and sandwiches style which can be chosen with different materials.

When the incident wave strikes on the surface of the dielectric, it is partially transmitted and a part of it is reflected back. Since a half-wave wall solid (monolithic) radome is studied in this thesis, reflection at normal incidence of a half-wave thick radome is shown in figure 2.2. In this figure, the electromagnetic wave radiated by the antenna enters the left wall of the radome. It is partially transmitted and partially reflected, where the transmitted wave travels a phase distance of 180° and hits the right radome wall, where it is partially transmitted and partially reflected with a phase shift of 180°. The reflected wave travels phase distance 180° inside the radome, and the process is repeated at the left wall. Summing up all internal reflections, it is seen that the transmitted waves at the right wall have the same phase and add constructively to maximum total transmission, whereas the waves at the left wall add destructively to yield zero total reflection. Figure 2.3 shows how a half-wave dielectric slab effects on EM waves that are incident to a radome wall with an oblique angle. During the transmission of an incident EM wave from the boundary, there exist reflection at the free-space/dielectric boundary and at

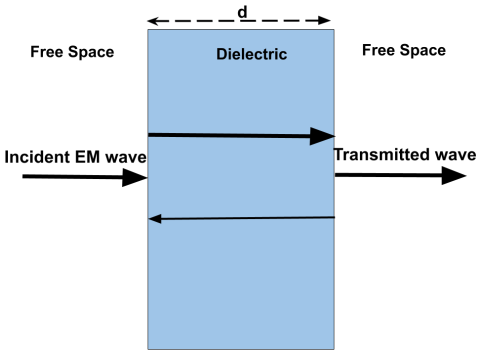

Figure 2.2: Reflection-transmission through a dielectric slab at normal incidence. Only the first two internal propagations are indicated.

the dielectric/free-space boundary. Multiple reflections and transmissions are not shown in this figure. A transmission without reflection can be achieved in the classical half-wave wall by constructive cancellation of reflected energy from each of the two boundaries [17]. The well-known half-wave thickness expression is for

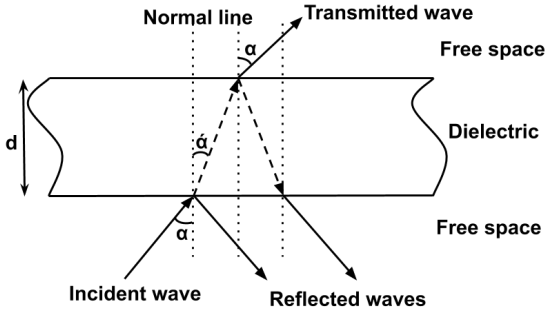

Figure 2.3: Reflection-transmission through a dielectric slab at an oblique incident angle.

constant thickness radome:

$$\lambda_0 = \frac{c_0}{f_c} \tag{2.2}$$

$$t = \frac{\lambda_0}{2\sqrt{\varepsilon_r}} \tag{2.3}$$

When considering the angle of incidence, the optimum thickness of the radome is given by (2.4) [18]:

$$t = \frac{\lambda_0}{2\sqrt{\varepsilon_r - \sin^2\theta}} \tag{2.4}$$

where,
c_0 = speed of light
f_c = resonating frequency
λ_0 = free space wavelength
t = radome wall thickness
ε_r = relative dielectric constant of radome material
θ = angle of incidence

After selecting material and calculating optimal thickness, designing the radome geometry is the next important stage to evaluate the impact of the radome on the antenna performance. As it is known, different shapes have different effects on wave propagation properties. Also different values for distance between antenna and radome cause different alternatives for each shape with different impacts on antenna performance boresight error, reflection coefficient, gain, etc.

Chapter 3

Implementation of Radome

Radomes can be manufactured in many shapes and sizes depending on the particular application. In this thesis, two geometries (Figure 3.1) were considered to evaluate the impact of radomes on antenna performance based on EM simulations. In this chapter, parameters and methodology of radome design for these alternatives are explained.

3.1 Parameters

The radome wall structure which is used in this design is the half-wave single layer wall due to its simplicity and having good RF performance. Table 3.1 shows all the parameters and expression of calculations in this thesis work.

Description	Parameter	Expression	Value
Design frequency	f_0		24 GHz
Design wavelength	λ_0	$\frac{c_0}{f_0}$	0.012427 m
Air permittivity	ε_0		1
Radome permittivity	ε_r		2.83
Radome loss tangent	$\tan\delta$		0.0076
Thickness of radome	t	$\frac{\lambda_0}{2\sqrt{\varepsilon_r}}$	0.0036934 m
Width of antenna	w	$7\lambda_0$	0.086986 m
Width of planar part of radome	W	w	0.086986 m
Distance from antenna to radome	d	$2\lambda_0$	0.024853 m
Radius of radome transition	r	λ_0	0.012427 m
Distance to far field surface*	R-ff	$6\lambda_0$	0.07456 m
Inner radius of PML*	R-pml1	$7\lambda_0$	0.086986 m
Outer radius of PML	R-pml2	$8\lambda_0$	0.099413 m

Table 3.1: Parameters of the radome and antenna design.
*The PML is a fictitious layer absorbing all outgoing waves, whereas the far field surface is where the fields are recorded and subsequently transformed to far field data by Comsol.

3.2 Geometry

Two different geometries (flat and curved) for the radome are designed. The shapes of these two geometries are presented in Figure 3.1. Different parameters for these two shapes were defined for each sub-geometry such as changing the distance of the antenna from the top and and edges of radome.

(a) Flat **(b)** Curve

Figure 3.1: Two different geometries for radomes.

3.3 Antenna configuration

Two different antenna models are implemented. A single port was a good choice as a planar antenna in the first step due to its simplicity. The waves of the electric field (E) for a single port antenna which is supposed to radiate in different angles from 0 to 75 degree were generated by the equation (3.1):

$$E = e^{-jkx\sin(\theta)} \tag{3.1}$$

The evaluation is based on applying equation (3.1) in the antenna aperture to the z-component or x-component to propagate wave in a single port design. To design the second alternative of antenna an array dipole antenna is considered. An antenna array is composed of two or more antenna elements that can be placed in different geometries such as linear, circular, spherical and etc [19]. In a linear antenna array, antenna elements are placed along one axis. The antenna array generates a beam that can be controlled by changing the geometry and also by other parameters, such as inter-element spacing, excitation amplitude and excitation phase of the individual element [20]. In this thesis this array antenna is designed in fourteen half wave dipole elements with half-wavelength separation between elements and quarter-wavelength height from ground-plane. The steering angle of the array antenna was calculated by changing the phase from the equation (3.2).

$$\alpha = -jkxsin(\theta) \tag{3.2}$$

Figure 3.2 shows a fourteen dipole array antenna.

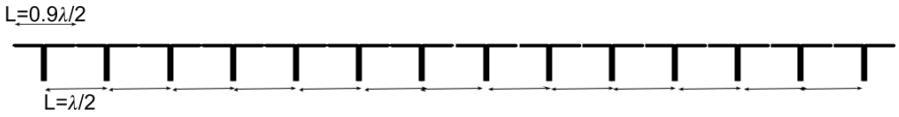

Figure 3.2: Array dipole antenna.

3.4 Evaluation method

After defining the parameters and antenna models, radomes were designed and simulated in Comsol Multiphysics for different alternatives. Then, some important parameters such as BSE, reflection coefficient and gain of these designs were calculated and compared by plotting in Matlab. Far field data was automatically computed in Comsol by selecting the far field boundaries and was available as a function of the angle in post processing. A refined mesh was defined at the far field boundary in order to improve the resolution in BSE. As mentioned before, BSE is one of the most important parameters to study how a radome effects on antenna performance. Additionally, radiation pattern in a steering angle were also plotted to see the effect of the radome on the main lobe and side-lobes of two antenna models. Figure 3.3, shows the BSE concept in case of a radome attached antenna and presents deviation of detected angle from actual angle [21]. To compute the BSE from Comsol data, the peak direction of the main lobe was evaluated with and without the radome by introducing a Comsol operator finding the maximum of an entity along the far field surface.

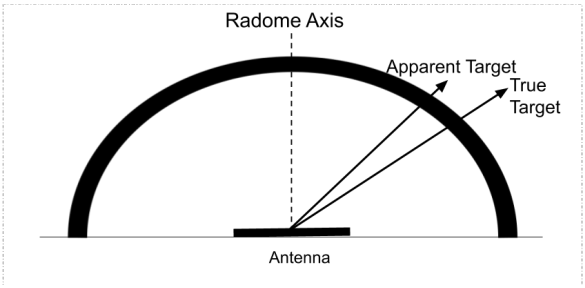

Figure 3.3: Graphic representation of Boresight error.

Chapter 4

Flat radome geometry

In this chapter, results of simulations and plots for the flat radome geometry enclosing two types of antennas; single-port antenna and 14-array dipole antenna are shown. The BSE for both antenna types and gain and reflection coefficient for single-port antenna are plotted in two polarizations, z-component and x-component and for different beam-steering angles from 0 to 75 degree. For the flat radome geometry, two parameters including distance of the antenna from the top of the radome (D) and from the edge of the radome on the ground plane (R) are changed to study the influence of these two parameters on the radiation pattern. These two distances are shown in Figure 4.1. Another factor that was implemented in our design is the shape of the radome's edge. Two geometries are considered as is shown in Figure 4.2. By changing these three parameters, nine alternatives (summarized in Table 4.1) were designed and simulated. Boresight error, gain and reflection coefficient are calculated to compare different designs and geometries.

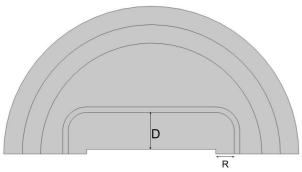

(a) Flat radome with a one port antenna.

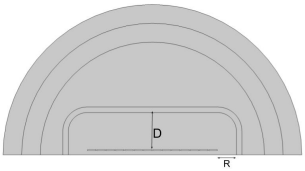

(b) Flat radome with a 14-array-dipole antenna.

Figure 4.1: Figure shows D and R that are changed to evaluate different designs.

Code	FR1	FR2	FR3	FR4	FR5	FR6	FR7	FR8	FR9
D	d	d	d	d/2	d/2	d/2	d/4	d/4	d/4
R	r	r/2	r/2	r	r/2	r/2	r	r/2	r/2

Table 4.1: Table of different values for two parameters D and R (Flat radome). $d = 2\lambda$ and $r = \lambda$.

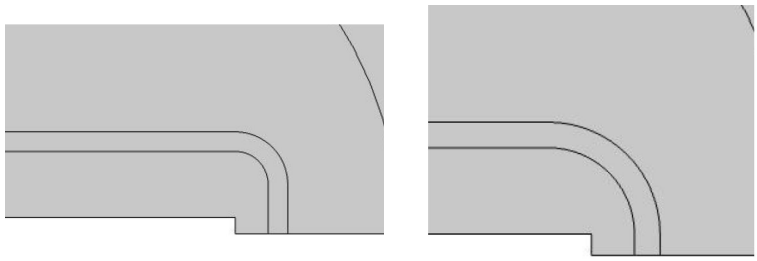

(a) Geometry of the flat radome edge A

(b) Geometry of the flat radome edge B

Figure 4.2: Different edge shapes for the flat radome.

4.1 Flat radome effect on a single-port antenna

Figures 4.3 and 4.4 present BSE for nine different designs. Each colour shows a constant distance of the antenna from the top of the radome. For beam-steering angles below 40 degree BSE is below 0.5 for nine designs. For beam steering angle larger than 40 degree, the curves have different BSE at different steering angles. The dashed green curve (D=d, R=r) has two minima at 44 degree and 50 degree. The BSE increases from zero to 5.0 when steering angle increases from 50 to 60 degree. The solid green curve has nearly similar behaviour as dashed green curve. When D decreases to d/2, the red curves show similar pattern while there is significant difference when r is varying. The lowest BSE for D=d/2 is for R=r/2 and B edge. When D decreases to d/4, the BSE tends to increase gradually when the beam steering angle increases.

By looking at BSE values in the Figure 4.4, we can see beam-steering angles below 40 have the same behaviour as the z-component and the BSE stays below 0.5, then starts to increase. The BSE of the green and red curves have a peak around 2 and 1.5, respectively, and then green curves go down below 1 and red curves below 0.5. Black curves have their BSE value below 1 until steering angle 58 degree then increase to 5 when the steering angle reaches 70 degree.

Figures 4.5 and 4.6 show the gains in z-component and x-component when there is no radome in place and when there is a radome with different designs. In Figure 4.5, similar to BSE, for beam-steering angle below 40 degree, all curves follow similar pattern. The blue curve indicating no radome present around the antenna has higher gain which confirms expectations. The gain decreases when the steering angle increases and minimum gain is 13 dB when there is not any radome present. After 40 degree, gains are different for different radomes. Two parameters of D and R are changing but as can be seen from the Figure 4.5, the R variations have no effect on the gain for z-component, while changing D has impact for the steering angle higher than 40 degree. The gain difference of the antenna with and without radome is maximum 2 dB for z component. Figure 4.6 presents

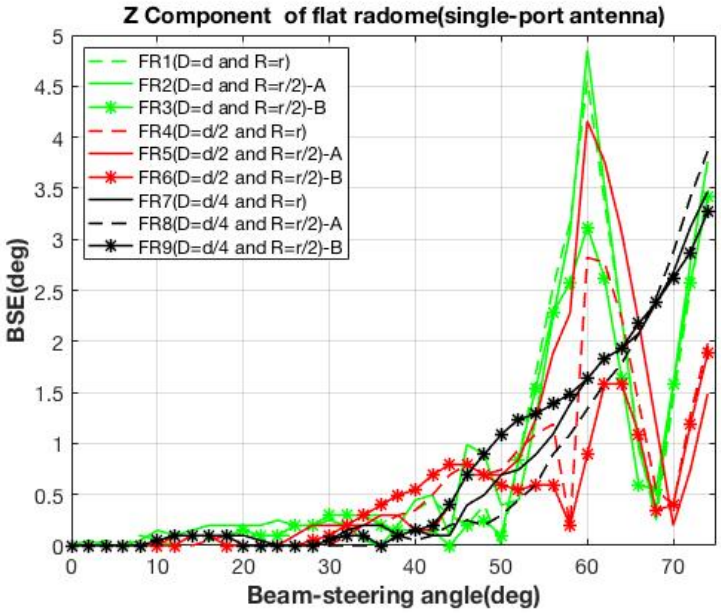

Figure 4.3: BSE of different alternatives of flat radome (single-port antenna) in z-component.

the gain of the antenna in the x-component polarization. It is obvious that all the curves follow the antenna gain which is shown with blue curve. Neither R nor D variations affect the gain in this component. The gain of ntenna without radome drops in x-component more than z-component when beam-steering angle increases.

Figures 4.7 and 4.8 show the reflection coefficient (S11) versus the beam steering angle. Reflection coefficient is very low at z-component and for x-component at low angles. It means that the antenna is well matched and there is not a reflection from the radome back to the antenna unless for high angles in x-component. By looking at Figure 4.7 it is obvious that the only parameter that has an influence (z-component) is the distance between the antenna and the top of the radome (D), while the distance between the edge of the radome to the antenna (R) has no impact on the reflection coefficient. The blue curve presents the reflection coefficient when the radome is not enclosed. When D=d is equal to 2λ, the green curves have different reflection coefficient at different angles. At 22 degree and 48 degree and above 68 degree the reflection coefficient is similar to the case without the radome present. When D=d/2 equal to λ, the S11 is at maximum for 52 degree steering angle and it decreases for degree above 52. For D=d/4 equal to $\lambda/2$, the reflection coefficient increases proportional to the steering angle and reaches to above -10 dB for steering angle above 60 degree. As is shown in Figure 4.8 all curves almost follow blue curves which presents reflection coefficient of the antenna without radome for the x-component with a difference around 2 dB from 5 degree to 40 degree. The curves have the same reflection coefficient to the blue curve after 40 degree.

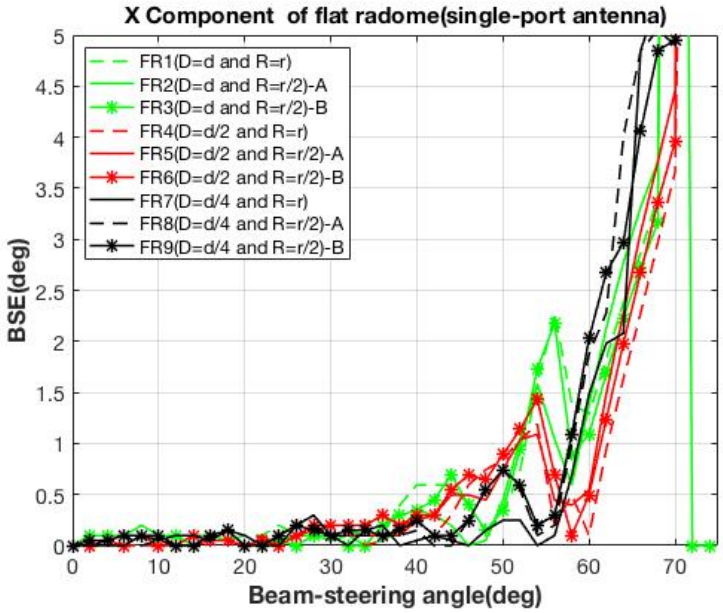

Figure 4.4: BSE of different alternatives of flat radome (single-port antenna) in x-component.

The radiation pattern plots of beam-steering angle in 70 degree in z-component and x-component, for some curves (FR1, FR4, FR5, FR6, FR9) are plotted in Figure A.1 and A.2 in Appendix A.

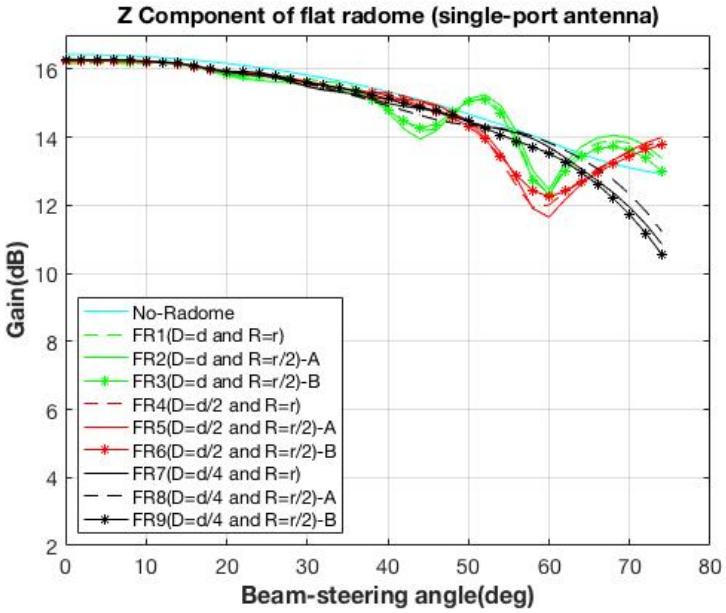

Figure 4.5: Gain of different alternatives of flat radome (single-port antenna) for z-component.

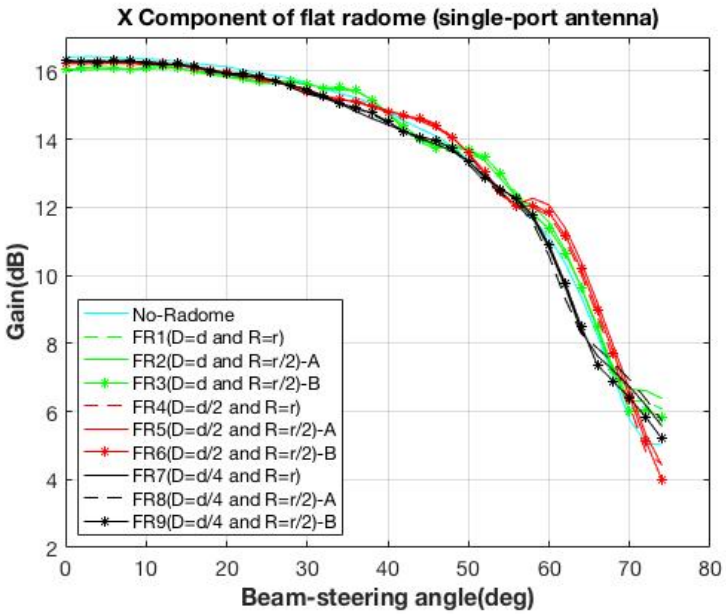

Figure 4.6: Gain of different alternatives of flat radome (single-port antenna) for x-component.

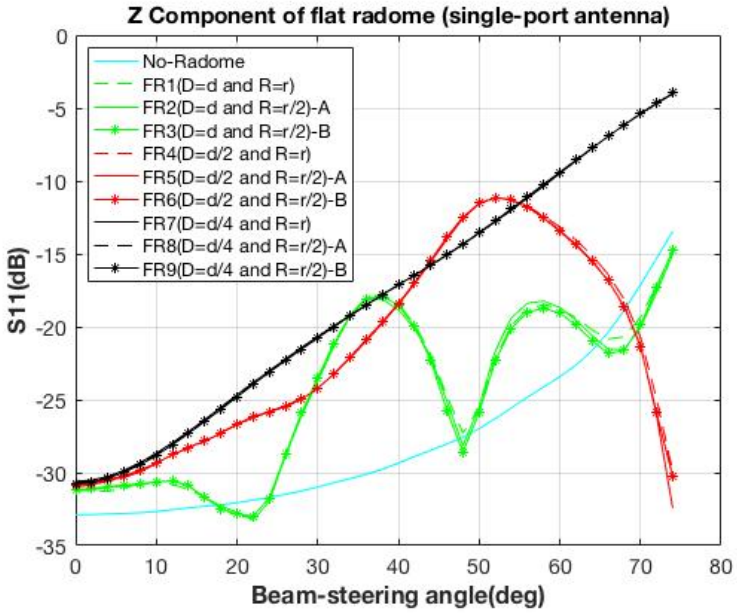

Figure 4.7: Reflection coefficient of different alternatives of flat radome (single-port antenna) for z-component.

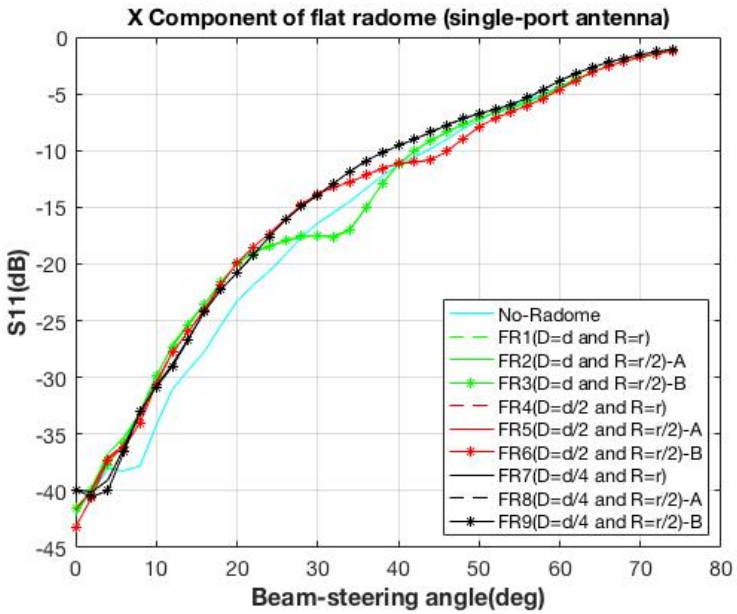

Figure 4.8: Reflection coefficient of different alternatives of flat radome (single-port antenna) for x-component.

4.2 Flat radome effect on an array-dipole antenna

In this section, all the radome design settings are similar to the previous design as explained in Table 4.1 but for a 14-array-dipole antenna which is shown in Figure 4.1b. For array-dipole antenna BSE are plotted in Figures 4.9 and 4.10 for nine different alternatives in both z-component and x-component. In Figure 4.9 the BSE is below 0.5 for all curves at beam-steering angles below 40 degree. For beam-steering angle larger than 50 degree, curves have different BSE. There are peaks at 60 degree for green curves where D=d, solid red curve and dashed red curve when D=d/2 and in 62 degree for star-red curves. Then BSE of all these curves drop and reach below 1 for BSE in 70 degree of beam-steering angle. Black curves follow BSE value below 1 till 48 degree then start to increase more linearly than other curves. In Figure 4.10 BSE of different alternatives of the flat radome enclosing an array-dipole antenna for the x-component polarization are plotted. All curves follow each other and BSE is below 0.5 util 40 degree of beam steering angle. Then the green curves and red curves when D=d and D=d/2, respectively, show a high peak and low peak between 50 and 60 degree of beam steering angle, and start to increase again and reach to BSE between 2.6 and 4 for 74 degree of beam-steering angle.

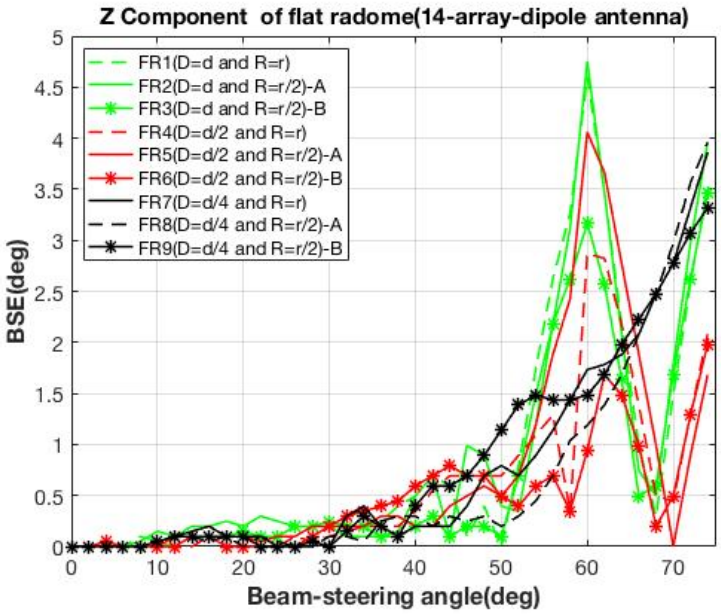

Figure 4.9: BSE of different alternatives of flat radome (14-array-dipole antenna) for z-component

Gain or reflection coefficient results are not presented for the array-dipole antenna due to the difficulty of handling many ports in Comsol. Therefore, it was decided to only extract far field data for array-dipole antenna model. Radiation pattern plots of flat radome effects on array-dipole antenna for beam-steering angle

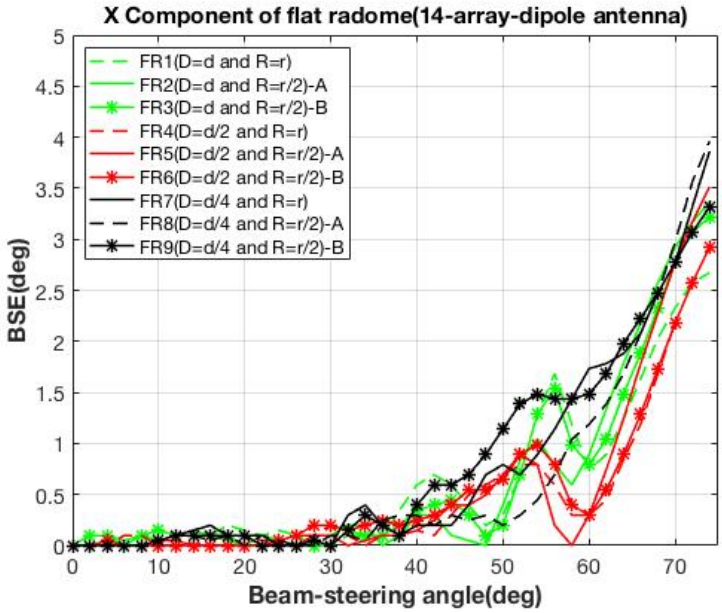

Figure 4.10: BSE of different alternatives of flat radome (14-array-dipole antenna) for x-component

70 degree for z-component and x-component are shown in Appendix A. These plots are for FR1,FR4,FR5,FR6 and FR9 designs.

Chapter 5

Curved radome geometry

For the curved radome geometry, six designs were simulated by changing two parameters (D) and (R) shown in Figure 5.1 and summarized in Table 5.1.

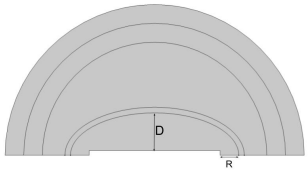

(a) Curved radome with a single-port antenna.

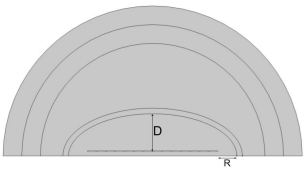

(b) Curved radome with a 14-array-dipole antenna.

Figure 5.1: Geometry and parameters D and R for curved radome designs.

Code	CR1	CR2	CR3	CR4	CR5	CR6
D	d	d	d/2	d/2	3d/2	3d/2
R	r	r/2	r	r/2	r	r/2

Table 5.1: Table of different values for two parameters D and R (curve radome with a single-port antenna) $d = 2\lambda$ and $r = \lambda$.

5.1 Curved radome effect on a single-port antenna

Figure 5.2 shows BSE of a curved radome enclosing a single-port antenna versus steering angles for the z-component polarization. The green curve is for D=d while the solid green curve represents the R=r and the dashed green curve shows the R=r/2. For D=d, the BSE value is low when R=r/2 and more significant for steering angles higher than 62 degree. When D is reduced to d/2, The BSE has higher value for R=r and it increases when R is increased to r/2. When D=3d/2 (purple curve), the BSE has the average lower value for D=3d/2 and is

maximum between 50 and 60 degree. BSE is very low at 66 degree. For steering angle higher than 70, the BSE increases for all designs except when D=d and R=r/2. The purple curves which correspond to the largest distance between the antenna and the radome have BSE less than 1.5 for beam-steering angles below 70 degree. This design also has nearly zero BSE for 64 and 66 beam-steering angle.

By looking at Figure 5.3 all curves follow each other and the BSE value increases gradually in six designs. However, BSE is lower than 1 until 40 degree and it increases to 3.5 for red curve which has the higher BSE after 50 degree. Purple curve has lowest BSE below 1.5 for the entire range.

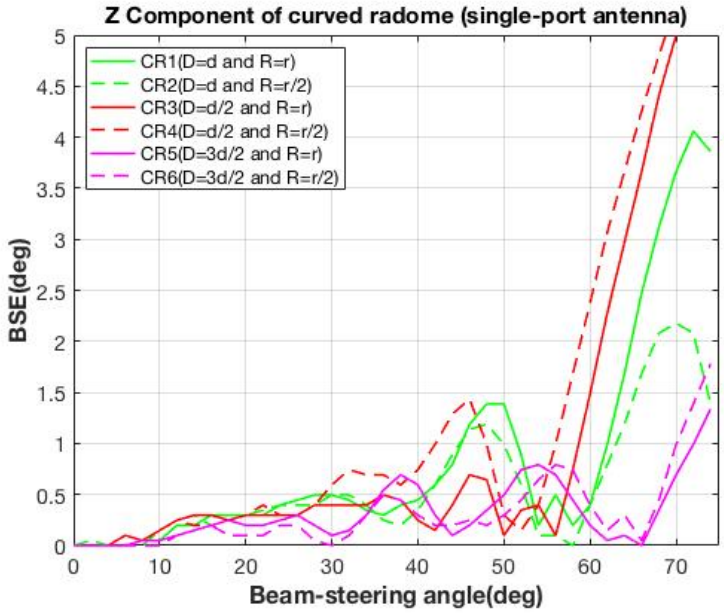

Figure 5.2: BSE of different alternatives of curved radome (single-port antenna) in z-component.

Figure 5.4 shows the gains at z-component polarization for different curved radome designs including when there is no radome present (blue curve). All curves almost follow the gain of the unenclosed antenna with a small fluctuations in gain values.

With regard to Figure 5.5 it is obvious that all curves follow the blue curves (no radome) which means that gain in x-component is the same as the antenna gain without radome for all beam-steering angles.

The reflection coefficient for all of the alternatives for z-component are shown in Figure 5.6. It is clear that all curves with the same D and different R have almost same behaviour but with different values. However, the differences between solid line and dashed line for red curves and green curves are higher than for the purple

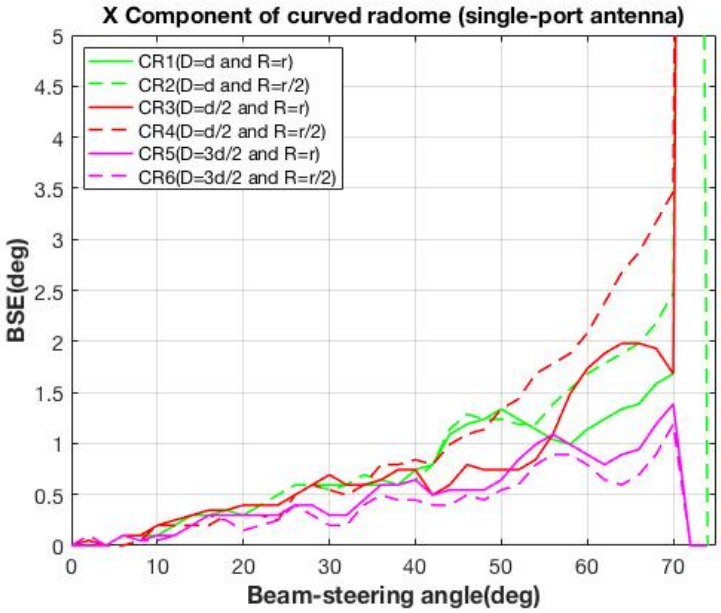

Figure 5.3: BSE of different alternatives of curved radome (single-port antenna) in x-component.

curves. Among different designs, red curves (D=d/2) has highest reflection for steering angles more than 40 degree. Green curve has a drop at reflection after 60 degree. Figure 5.7 shows all curves almost follow blue curves which presents reflection coefficient of the antenna without radome for the x-component with a small difference until 50 degree. Then all curves have same reflection coefficient to the blue curve. After beam steering angle 40 degree, all curves have reflection coefficient around -10 db and 0 same as antenna behaviour.

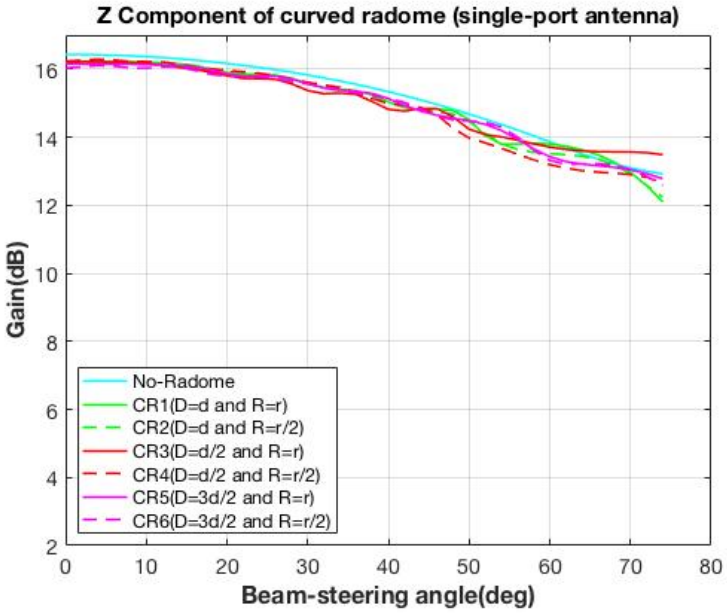

Figure 5.4: Gain of different alternatives of curved radome (single-port antenna) in z-component.

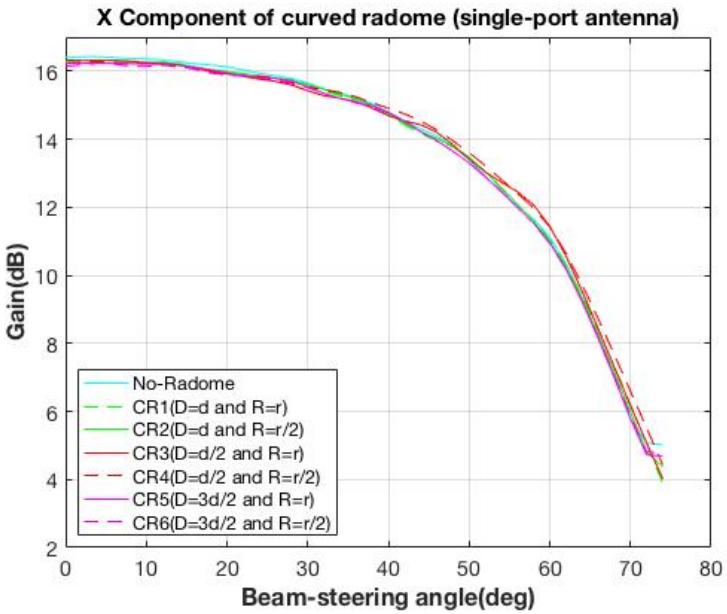

Figure 5.5: Gain of different alternatives of curved radome (single-port antenna) in x-component.

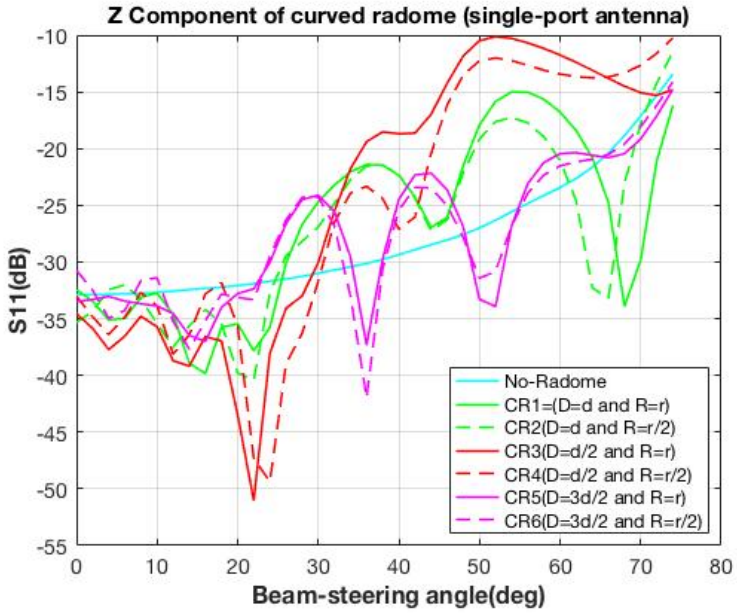

Figure 5.6: Reflection coefficient of different alternatives of curved radome (single-port antenna) in z-component.

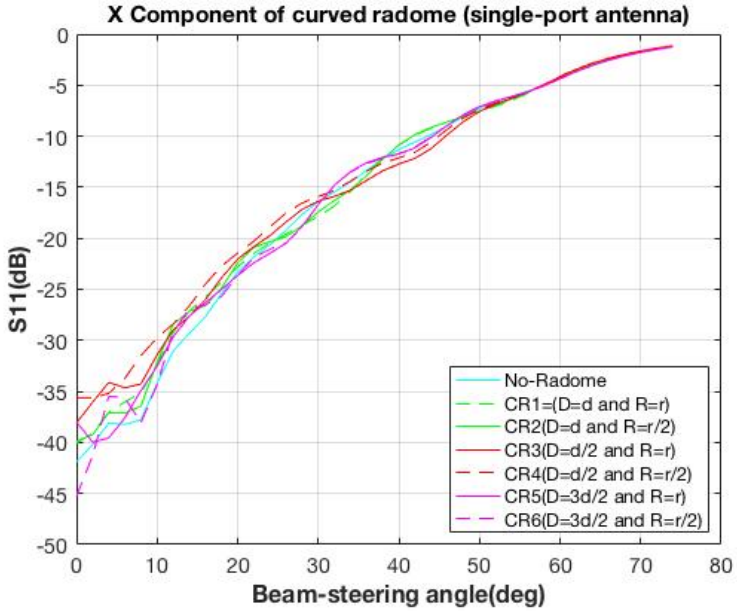

Figure 5.7: Reflection coefficient of different alternatives of curved radome (single-port antenna) in x-component.

Radiation patterns of curved radome enclosed to single-port antenna are plotted for a certain steering angle in Figures A.5 and A.6 for z-component and x-component respectively.

5.2 Curved radome effect on an array-dipole antenna

Figure 5.8 presents BSE of different alternatives of curved radome for a 14-array dipole antenna with changing two parameters as explained in Table 5.1 for z-component. All curves have BSE less than 1 before 40 degree. The BSE increases to 1.5 for green curves when D=d and for dashed red curve when D=d/2 and R=r/2. BSE is near 0.5 for solid line with parameters D=d/2 and R=r between 40 and 50 degree. The BSE value for all designs is below 1 for angle between 50 and 54. The BSE value remains lower than 1.0 for purple curves until 70 degree. Other designs tends to provide a large BSE value for beam steering angle higher than 60 degree. By looking at BSE values for x-component in Figure 5.9 we can see all curves keep BSE value bellow 1 until beam steering angle 42 degree. Then dashed red curves increase until 3 in 74 degree where red and green solid curves have maximum BSE value 2 in 74 degree. The green dashed curve has BSE around 1 for most beam steering angle after 42 degree except in 60 degree which has a small increase until 1.3 for BSE value. Purple curves have BSE value below 1 for all beam steering angles.

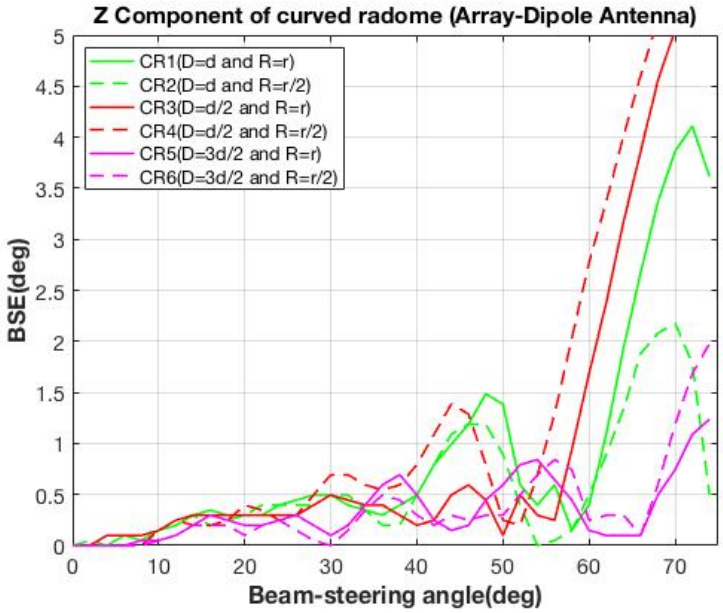

Figure 5.8: BSE of different alternatives of curved radome (14-array-dipole antenna) in z-component.

Radiation patterns of all curves for curved radome enclosing an array-dipole

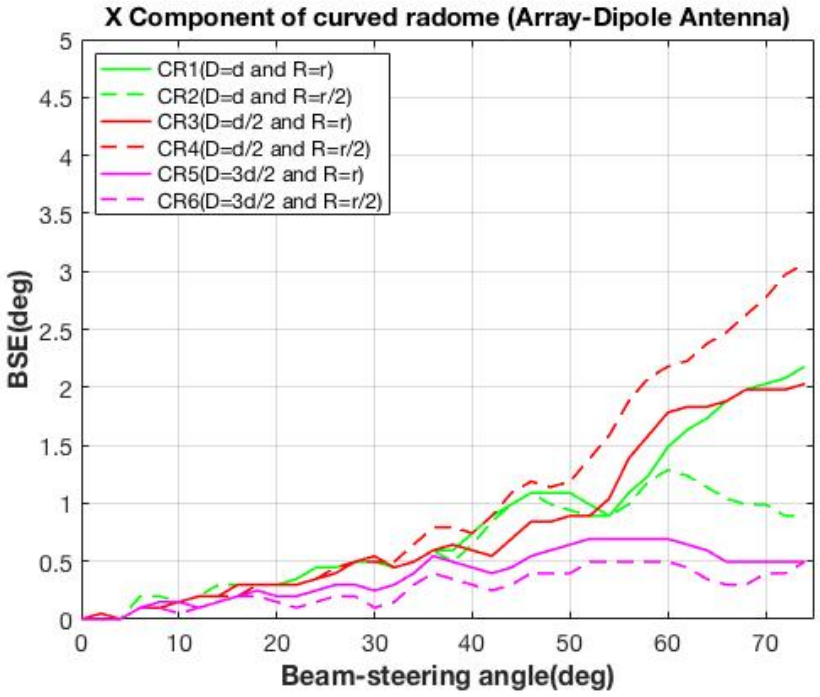

Figure 5.9: BSE of different alternatives of curved radome (14-array-dipole antenna) in x-component.

antenna are plotted in Figures A.7 and A.8 in Appendix A for z-components and x-component.

Chapter 6

Discussion and conclusion

The aim of the thesis is to quantify the effect of the radome on the antenna performance, focusing on different geometries at 24 GHz, 24.125 GHz and 24.25 frequency and a certain material. There was not any significant deviation in results for different frequencies. Therefore, the results for 24 GHz are presented in this thesis. The antenna was modelled in the Comsol Multiphysics software. The radome was added to the design and wave propagation from the antenna was simulated in different steering angles in range of 0 to 75 degree in two degree steps. The degradation of the radiation characteristic of the antenna was evaluated by calculating the gain loss, boresight error (BSE) and reflection coefficient (S11). The sidelobe level variation was also assessed which can be represented by distortion of the radiation pattern. In order to minimize the degradation of radiation which is the golden goal of this thesis, a few geometrical parameters including the distance of the antenna from the top of radome and from the edge of the radome on the ground plane were altered. Attempts were made to apply some absorbing material at the edges of the radome to reduce scattering, but no immediate improvement was observed and no further investigation was made.
Two antenna models including a single-port antenna and an array-dipole antenna were implemented. The first step was to evaluate the distortion of the radiation pattern caused by the radome on two different types of antenna. To accomplish that, the BSE was retrieved in z-component and x-component polarization for the flat radome design and the curved radome, in both cases with two different antennas enclosed. Figures 4.3 and 4.9 present the BSE for z-component and indicate a very similar pattern for the two antenna models with slight difference in 72 and 4 degree for solid red curves and between 40-50 degree for star and solid black curves. However, when looking at the BSE values for the x-component in Figure 4.4 and 4.10, it can be seen that the radome has different effect for the two antenna models. This difference is significant for steering angle larger than 60 degree. In a similar approach, the BSE was calculated for the curved radome for single-port and array-dipole antenna. Similar to the flat radome, there is not a distinction in BSE for z-component while a notable difference in x-component for angle larger than 70 degree.
The radiation patterns for z-component for steering angle 70 degree are plotted in figures A.1 and A.3 to provide additional information on wave propagation. Result from visual diagnosis of radiation pattern coincides with BSE variations meaning that if there is not any deviation in main lobe, the BSE is very low. The radiation

patterns show that the more realistic array-dipole antenna has more problems with sidelobes, and needs to be carefully designed.
What can be discussed at this point is the high BSE for large steering angles. This significant BSE can to some extent be restrained by radome design. It can be seen from the BSE plots that parameter variations cause changes in BSE. The next step is to compare different designs in each radome to evaluate the radome's performance on wave radiation from antenna. In this step, the single-port antenna was selected as source of radiation. The main reason for this selection is that the radome's performance can be evaluated using BSE, gain and reflection coefficient. It is not feasible to calculate the gain for an array antenna, since the model contains a large number of separate ports which cannot easily be combined. BSE of different designs are plotted for flat radome in Figure 4.3. For the z-component, when D=d, the BSE value is high for large angles. The optimal design considering BSE is when D=d/2 and R=r/2 and for the flat radome with more extension in the Figure 4.2b, when BSE is below 2 in all angles. Interestingly, the designs with D=d/4 have a smooth increase when the steering angles is getting larger. However, the BSE is more than 2 for angles above 64 degree. The result for gain at z-component shows fluctuations in data for the design with D=d and d/2 while the design with D=d/4 illustrates less variation in gain.

Since there is not a significant coherence between BSE and gain results, one can consider two scenarios and interpret data for a certain application. For instance, if directionality at high steering angle is the main scope of the application, FR6 design can be a good choice in parameters. In another scenario, if range sensitivity is the key, gain plot can provide desired information. However the gain plot in Figure 4.5 in z-component shows that red and green curves oscillate undesirably and further consideration to retrieving a smooth gain variation is needed.

The reflection coefficient was analyzed for various designs in both radomes. Similar to gain results,the reflection coefficient of the antenna with the flat radome oscillates in z-components more than x-component. For x-components it tends to be more linear with small variation in different designs. The reflection coefficient is typically very small for the single-port antenna model, and only gives hints on the radome performance. In these designs, gain difference is not very significant and the most important metric is BSE.

One parameter that was implemented in the flat radome was the design of different edge geometries. When other parameters are constant and the only alternation is the edge geometry, there is still a significant variation in BSE.

The two scenarios can be considered for the curved radome when six designs show BSE and gain at different angles. For the curved radome, when D=3d/2, BSE is below 1.5 for the entire steering angle range for both components. Gain curves are more reasonable and show smooth decrease for both components. The reflection coefficient shows similar results to flat radome.

In conclusion, to provide a reasonable design for a radome, the radiation char-

acteristics comparison of an antenna enclosed in two different geometries is presented by a series of numerical simulations. The results propose that the best choice depends on the application that the radome is intended to be used in. Regarding direction-finding characteristic or range sensitivity, the height of the radome and the distance from the antenna edge to the radome wall can be selected. Comparing two geometries for one application, the curved radome has less fluctuation in evaluation parameters and has smoother gain variations. With respect to BSE, curved radomes CR5 and CR6 seem most promising candidates due to having a BSE in the order of 1 degree or less for most steering angles.

Chapter 7
Future Work

In this thesis two designs were considered for the edge of the flat radome. To extend this work, it will be interesting to investigate further designs for radome edge. Another area of interest for future work is to examine the effect of using absorber material in the radome to decrease the effect of the radome on the antenna performance in beam-steering angle more than 60 degrees, which was only briefly attempted in this thesis. By improving the agreement of these results, simulation tools such as HFSS can be used more effective and reliably to study the effect of these radomes on antenna performance and evaluation of the parameters which may be theoretically interesting but difficult to implement in practice. More evaluation in array-dipole antenna is also a factor that can be assessed to give a better understanding of this kind of antenna.

Appendix A

Radiation pattern plots

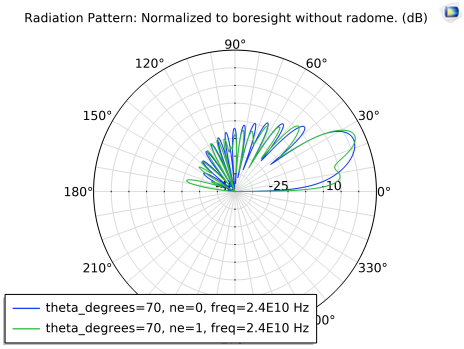

(a) FR1:70 degree-Z

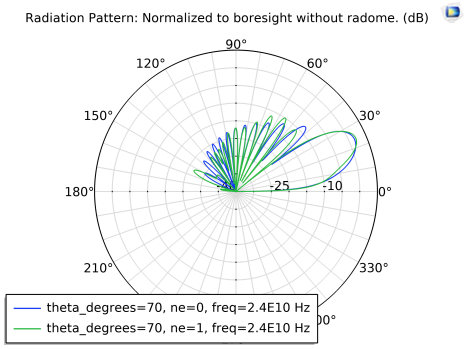

(b) FR4:70 degree-Z

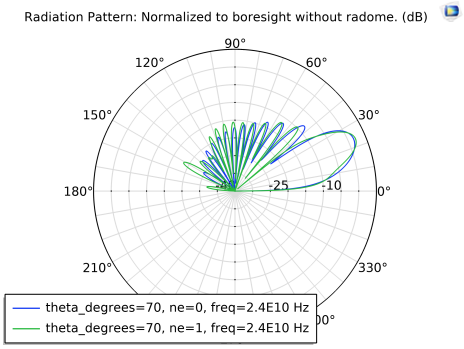

(c) FR5:70 degree-Z

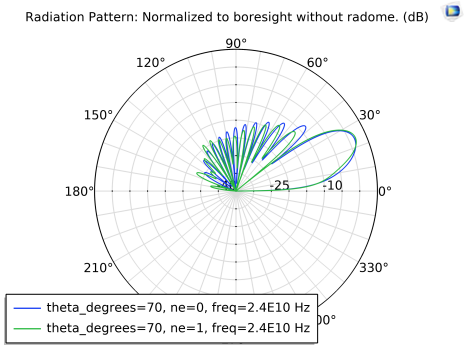

(d) FR6:70 degree-Z

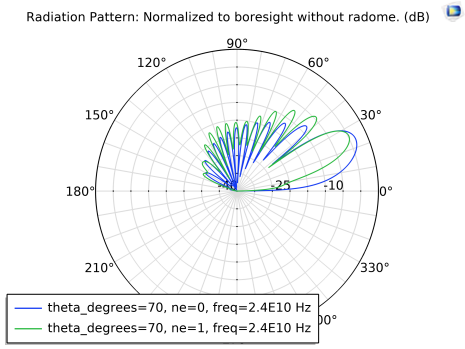

(e) FR9:70 degree-Z

Figure A.1: Radiation pattern plots of different alternatives of flat radome (single-port antenna) beam-steering angle 70 degree in z-component.

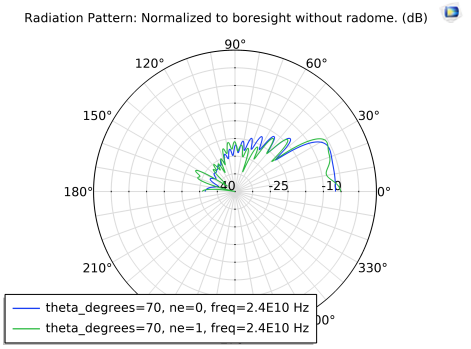

(a) FR1:70 degree-X

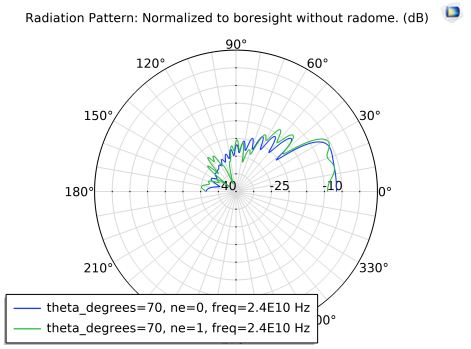

(b) FR4:70 degree-X

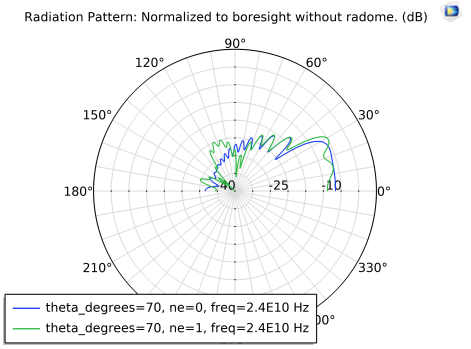

(c) FR5:70 degree-X

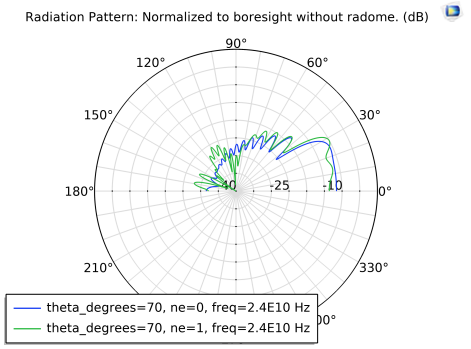

(d) FR6:70 degree-X

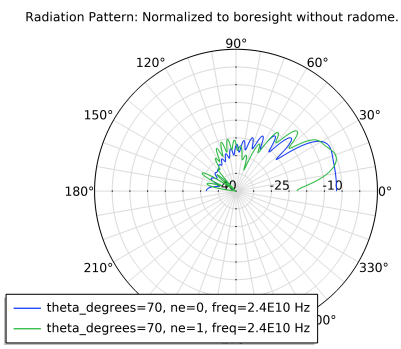

(e) FR9:70 degree-X

Figure A.2: Radiation pattern plots of different alternatives of flat radome (single-port antenna) beam-steering angle 70 degree in x-component.

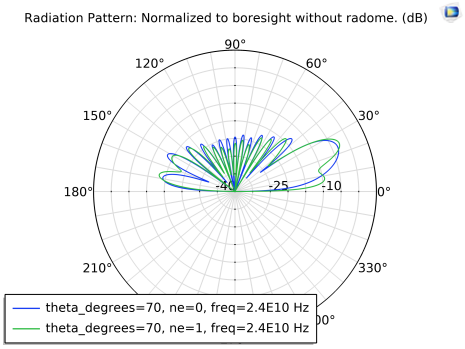

(a) FR1:70 degree-Z

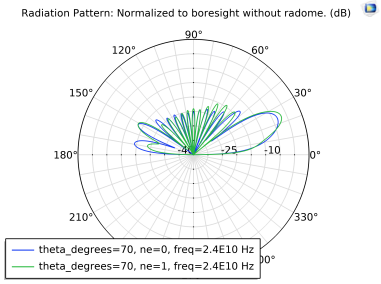

(b) FR:70 degree-Z

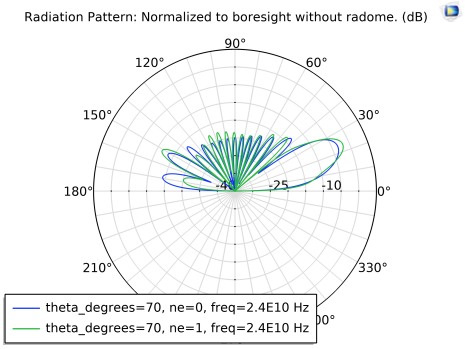

(c) FR5:70 degree-Z

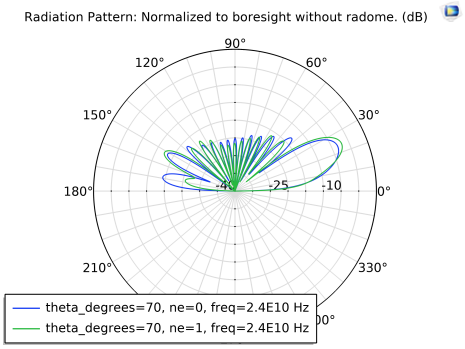

(d) FR6:70 degree-Z

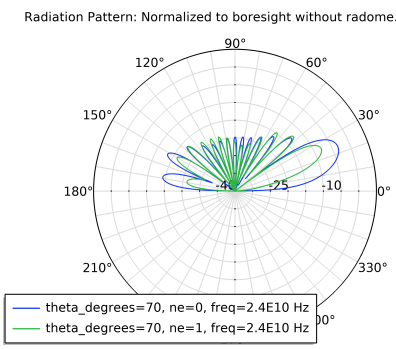

(e) FR9:70 degree-Z

Figure A.3: Radiation pattern plots of different alternatives of flat radome (array-dipole antenna) beam-steering angle 70 degree in z-component.

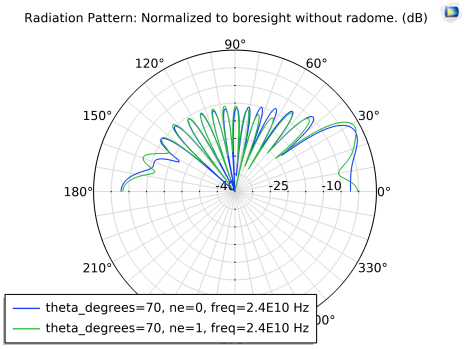

(a) FR1:70 degree-X

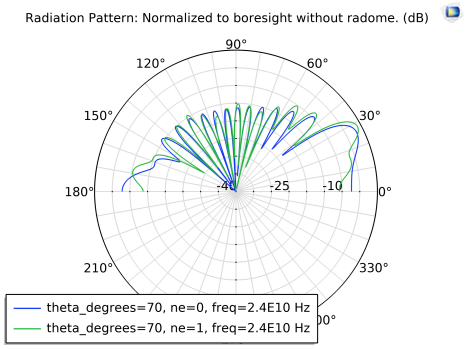

(b) FR4:70 degree-X

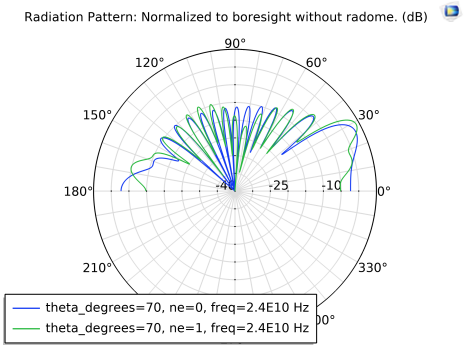

(c) FR5:70 degree-X

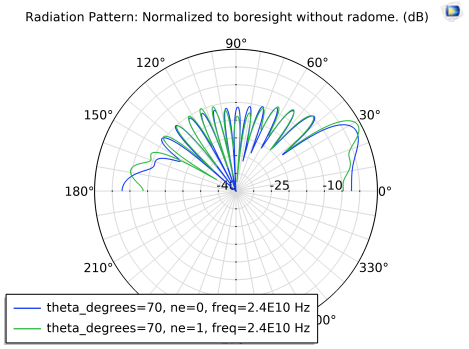

(d) FR6:70 degree-X

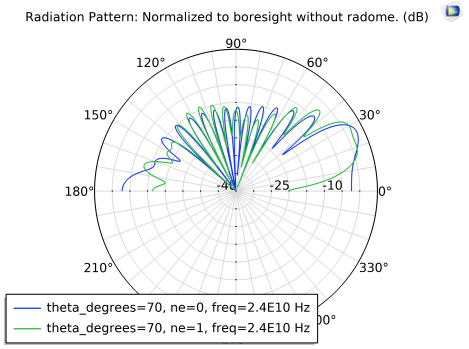

(e) FR9:70 degree-X

Figure A.4: Radiation pattern plots of different alternatives of flat radome (array-dipole antenna) beam-steering angle 70 degree in x-component.

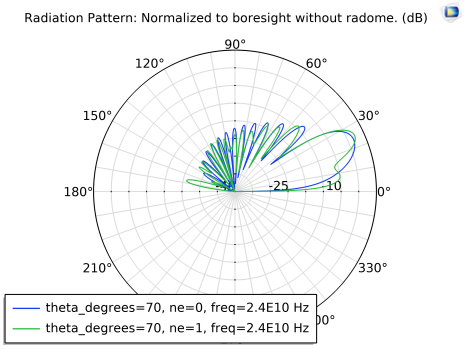

(a) CR1:70 degree-Z

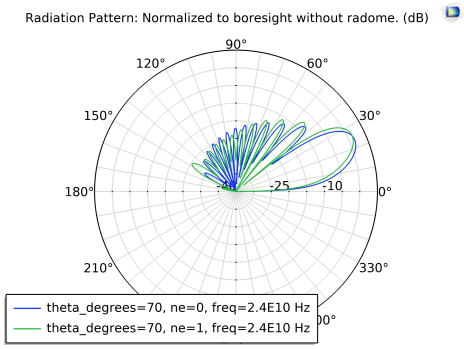

(b) CR2:70 degree-Z

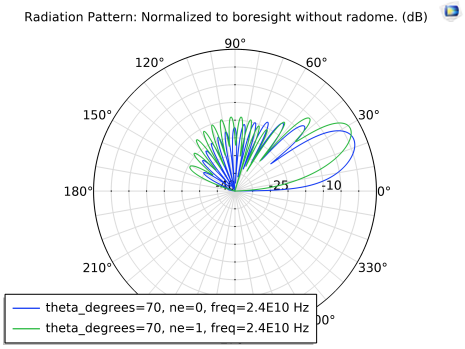

(c) CR3:70 degree-Z

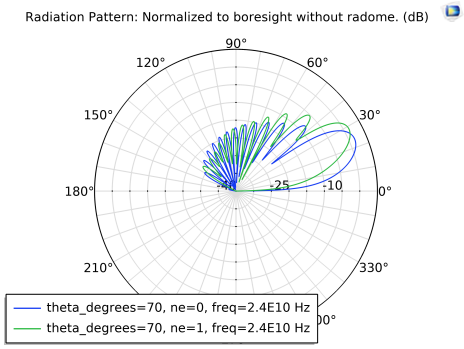

(d) CR4:70 degree-Z

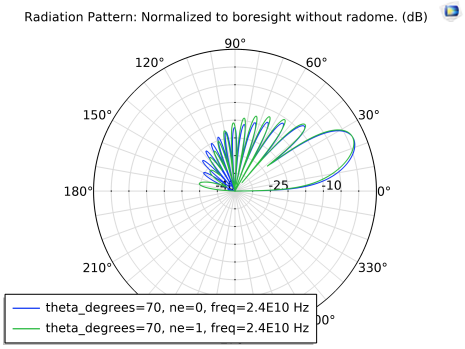

(e) CR5:70 degree-Z

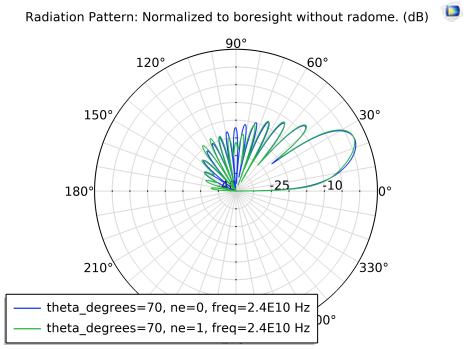

(f) CR6:70 degree-Z

Figure A.5: Radiation pattern plots of different alternatives of curved radome (single-port antenna) beam-steering angle 70 degree in z-component.

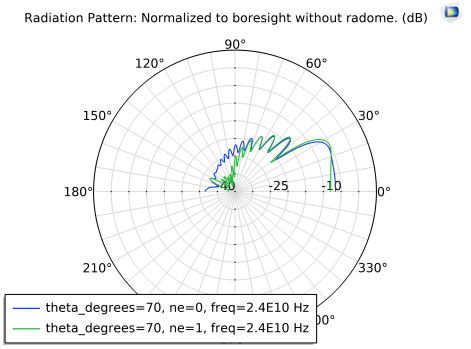

(a) CR1:70 degree-X

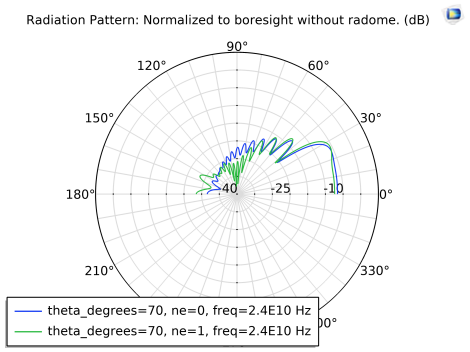

(b) CR2:70 degree$_X$

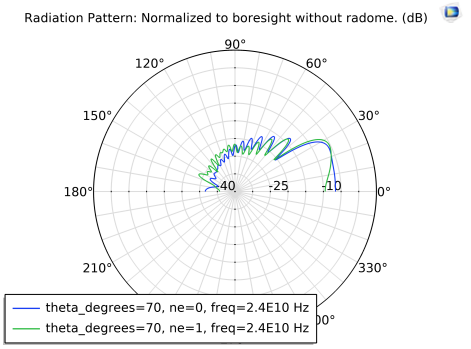

(c) CR3:70 degree$_X$

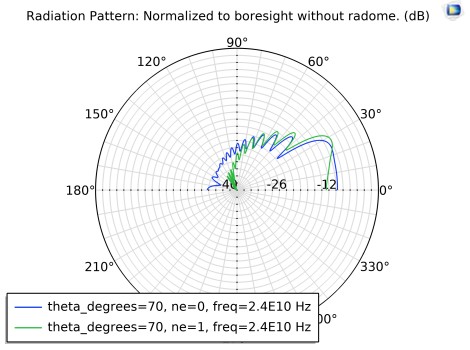

(d) CR4:70 degree-X

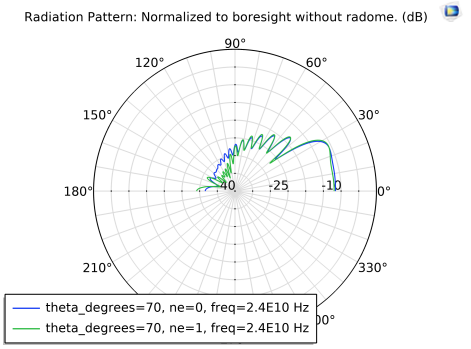

(e) CR5:70 degree-X

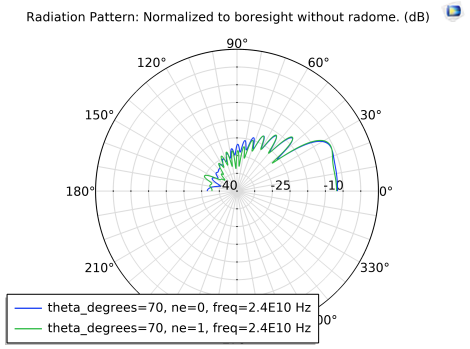

(f) CR6:70 degree-X

Figure A.6: Radiation pattern plots of different alternatives of curved radome (single-port antenna) beam-steering angle 70 degree in x-component.

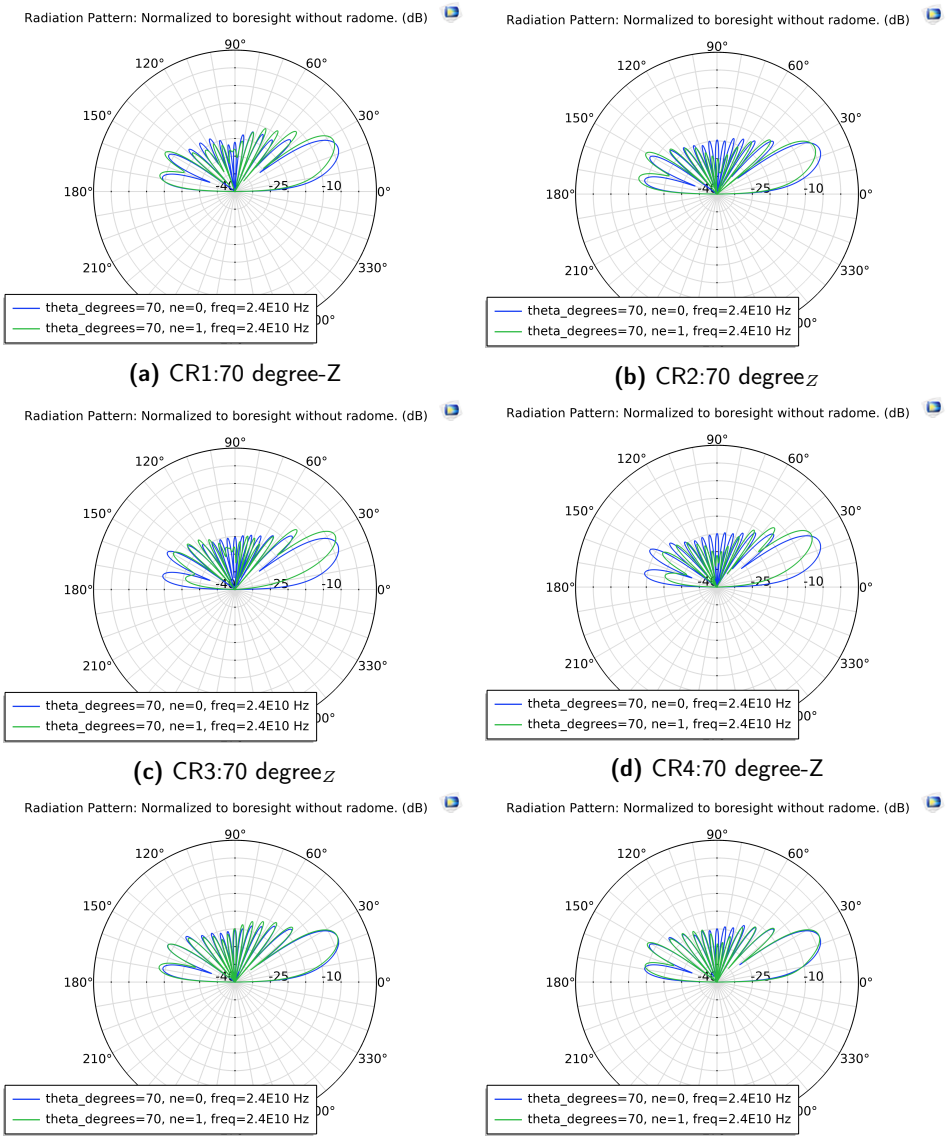

(a) CR1:70 degree-Z

(b) CR2:70 degree$_Z$

(c) CR3:70 degree$_Z$

(d) CR4:70 degree-Z

(e) CR5:70 degree-Z

(f) CR6:70 degree-Z

Figure A.7: Radiation pattern plots of different alternatives of curved radome (array-dipole antenna) beam-steering angle 70 degree in z-component.

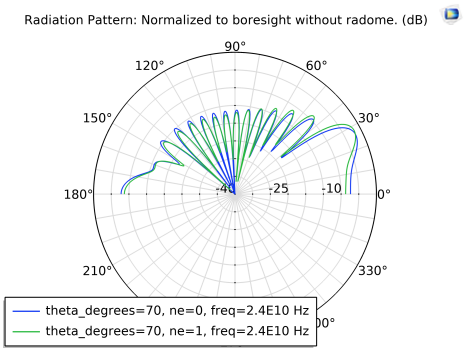

(a) CR1:70 degree$_X$

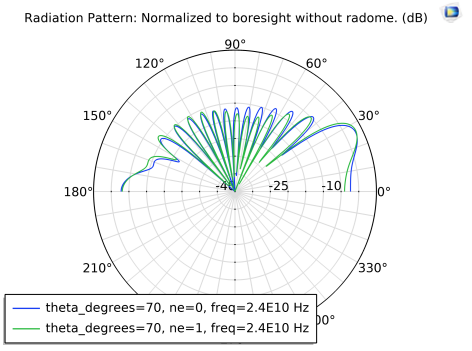

(b) CR2:70 degree-X

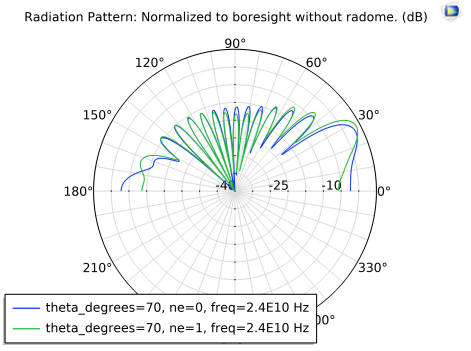

(c) CR3:70 degree-X

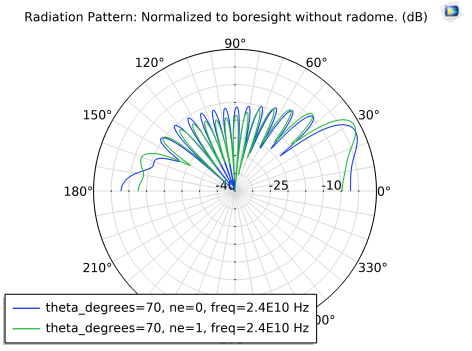

(d) CR4:70 degree-X

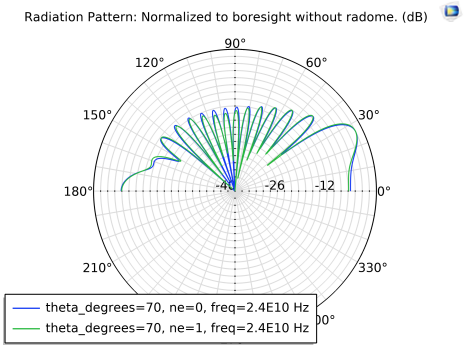

(e) CR5:70 degree-X

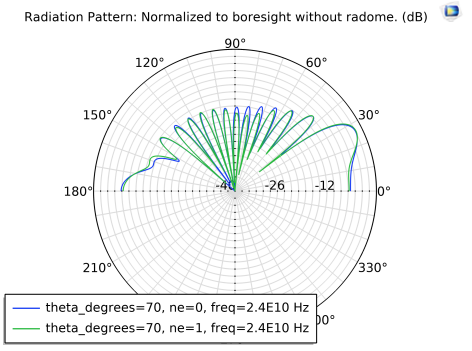

(f) CR6:70 degree-X

Figure A.8: Radiation pattern plots of different alternatives of curved radome (array-dipole antenna) beam-steering angle 70 degree in x-component.

Bibliography

[1] Mashury Wahab. "Radar radome and its design considerations". In: *International Conference on Instrumentation, Communication, Information Technology, and Biomedical Engineering 2009*. IEEE. 2009, pp. 1–5.

[2] Dennis J Kozakoff. *Analysis of radome-enclosed antennas*. Artech House, 2010.

[3] V Mercy Soumya et al. "Design considerations of radomes: a review". In: *International Journal of Mechanical Engineering and Technology* 8.3 (2017), pp. 42–48.

[4] Fang Hsu, P-R Chang, and K-K Chan. "Optimization of two-dimensional radome boresight error performance using simulated annealing technique". In: *IEEE transactions on antennas and propagation* 41.9 (1993), pp. 1195–1203.

[5] Hongfu Meng and Wenbin Dou. "Multi-objective optimization of radome performance with the structure of local uniform thickness". In: *IEICE Electronics Express* 5.20 (2008), pp. 882–887.

[6] Wanye Xu et al. "EM performance analysis of radomes with material properties errors". In: *IEEE Antennas and Wireless Propagation Letters* 13 (2014), pp. 848–851.

[7] Liu Li-Guo et al. "Design of an invisible radome by frequency selective surfaces loaded with lumped resistors". In: *Chinese Physics Letters* 30.6 (2013), p. 064101.

[8] Ning Liu et al. "A feasible bandwidth compensation technique for FSS radome design". In: *IEICE Electronics Express* 14.13 (2017), pp. 20170510–20170510.

[9] Alan W Rudge and K Milne. *The handbook of antenna design*. Vol. 16. IET, 1982.

[10] S Ilavarasu et al. "An approach to the design of composite radome for airborne surveillance application". In: *Technology* 9.2 (2018), pp. 36–48.

[11] Lance Griffiths and Radome Design Engineer. "A fundamental and technical review of radomes". In: *Microwave ProductDigest* (2008).

[12] Daniel David Barnard. "Bore Sight Error analysis in seeker antennas: A fully functional GUI interfaced Ray Tracing Solution". PhD thesis. Stellenbosch: Stellenbosch University, 2013.

[13] Erik G Geterud. "Design and Optimization of Wideband Hat-Fed Reflector Antenna with Radome for Satellite Earth Station". Chalmers University of Technology, 2012.

[14] Karl F Warnick, Ely Levine, and Haim Matzner. "IEEE publishes a revision of the standard for definitions of terms for antennas: educational kit for antennas and radiation [education column]". In: *IEEE Antennas and Propagation Magazine* 56.3 (2014), pp. 208–214.

[15] "IEEE Standard Definitions of Terms for Antennas". In: *IEEE Std 145-1993* (1993), pp. 1–32.

[16] Viktor Képeši and Ján Labun. "Radar Signal Attenuation due to Finite Radome Thickness". In: *NAŠE MORE: znanstveno-stručni časopis za more i pomorstvo* 62.3 Special Issue (2015), pp. 200–203.

[17] Wanye Xu et al. "A new efficient thickness profile design method for streamlined airborne radomes". In: *IEEE Transactions on Antennas and Propagation* 65.11 (2017), pp. 6190–6195.

[18] S Sunil et al. "A modified expression for determining the wall thickness of monolithic half-wave radomes". In: *Microwave and optical technology Letters* 30.5 (2001), pp. 350–352.

[19] Hubregt J Visser. *Array and phased array antenna basics*. John Wiley & Sons, 2006.

[20] Saeed Ur Rahman et al. "Analysis of linear antenna array for minimum side lobe level, half power beamwidth, and nulls control using PSO". In: *Journal of Microwaves, Optoelectronics and Electromagnetic Applications* 16.2 (2017), pp. 577–591.

[21] Nikhil Khatavkar and K Balasubramanian. "Composite materials for supersonic aircraft radomes with ameliorated radio frequency transmission-a review". In: *RSC advances* 6.8 (2016), pp. 6709–6718.

Printed by Tryckeriet i E-huset, Lund 2020

LUND
UNIVERSITY

Series of Master's theses
Department of Electrical and Information Technology
LU/LTH-EIT 2020-776
http://www.eit.lth.se